



# **Two-Dimensional Nuclear Analysis in Support of ITER Blanket Module Design**

**M.E. Sawan**

**May 2011**

**UWFDM-1393**

***FUSION TECHNOLOGY INSTITUTE  
UNIVERSITY OF WISCONSIN  
MADISON WISCONSIN***

**Two-Dimensional Nuclear Analysis in Support  
of ITER Blanket Module Design**

M.E. Sawan

Fusion Technology Institute  
University of Wisconsin  
1500 Engineering Drive  
Madison, WI 53706

<http://fti.neep.wisc.edu>

May 2011

UWFDM-1393

# Two-Dimensional Nuclear Analysis in Support of ITER Blanket Module Design

Mohamed E. Sawan  
Fusion Technology Institute  
University of Wisconsin-Madison  
Madison, WI 53706 USA  
sawan@engr.wisc.edu

## Abstract

**Detailed profiles of nuclear heating and radiation damage parameters were determined in ITER blanket modules at different poloidal locations. The results indicate that the nuclear parameters are sensitive to the configuration and material composition with enhanced steel heating and helium production in regions with large water content.**

## I. INTRODUCTION

The ITER blanket modules (BM) provide the main thermal and nuclear shielding of the vacuum vessel (VV) and external components. The BMs consist of a First Wall (FW) panel supported by a Shield Block (SB) [1]. The blanket system is also a plasma limiter and therefore its plasma-facing part (FW) is shaped to handle the plasma heat loads [2]. Each BM is attached to the VV through a mechanical attachment system of flexible supports and a system of keys. These BMs cover  $\sim 600 \text{ m}^2$  of the inner VV wall. Cooling water to the BM is supplied by manifolds supported off the VV behind or to the side of the SB. The BMs are arranged in the poloidal direction into 18 rows with rows 1-6 in the inboard region, rows 7-10 in the upper region and rows 11-18 in the outboard region. The lowest inboard module is designated as BM01 and the lowest outboard module is BM18. A total of 440 wall-mounted BMs, weighting  $\sim 4$  tons each, are used.

The FW panel consists of an array of plasma-facing fingers assembled with a toroidal orientation onto a stainless steel central support beam. Each FW finger includes beryllium (Be) armor, copper heat sink, and steel structure with embedded water coolant. Two types of heat sink are considered depending on the heat flux level at each poloidal location [1]. The normal heat flux (NHF) FW panels have steel (SS316-L(N)-IG) tubes embedded into a copper alloy (CuCrZr). The enhanced heat flux (EHF) FW panels employ CuCrZr rectangular or circular channels. The dimensions and composition of the FW panels are different for the NHF and EHF types. Thinner fingers with larger water content are used in the EHF FW panels. On the other hand, the water content is significantly higher in the beam and steel support zones of the NHF FW panels.

The design of the BMs is going through several iterations that include assessment of the stresses and performing detailed computational fluid dynamics (CFD) and electromagnetic analyses. This requires accurate knowledge of the volumetric nuclear heating due to neutrons and secondary gamma photons. To facilitate these analyses, we need to determine the nuclear heating in the FW panels and the SBs with sufficient spatial resolution. We started by performing 2-dimensional neutronics calculations to produce detailed nuclear heating profiles in each component separately (Be, Cu, SS, water) needed for thermal analysis. Calculations were performed for several EHF and NHF FW panels with their associated SBs. We used a simplified 2-D radial build and material composition based on the detailed CAD models for these designs. In addition, we determined the profiles of cumulative radiation damage (dpa) and helium production in the Cu and SS. This information is useful in assessing the impact on the mechanical properties and determining the expected lifetime for these structural elements. Re-welding is required at several locations in the BM and the VV behind it and the helium production results represent an important input for evaluating this issue.

In this paper, the results for several NHF and EHF BMs are presented. Assessment of the impact of various material compositions and configurations will be provided. While calculations were performed for BMs at nine different poloidal locations and results are being utilized in engineering analyses of these modules, we will report here the results for the inboard BM02 and outboard BM14 to illustrate the design effects. Fig. 1 shows the CAD model for the NHF FW02 panel and Fig. 2 gives the model for the EHF FW14 panel.

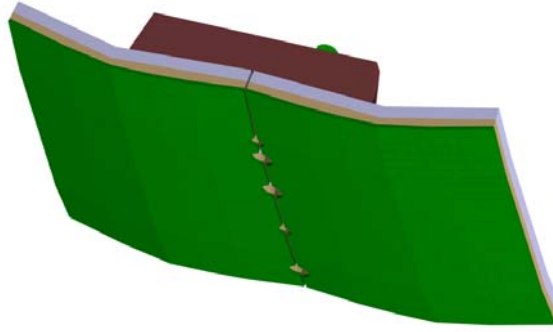


Figure 1. CAD model for the NHF FW02.

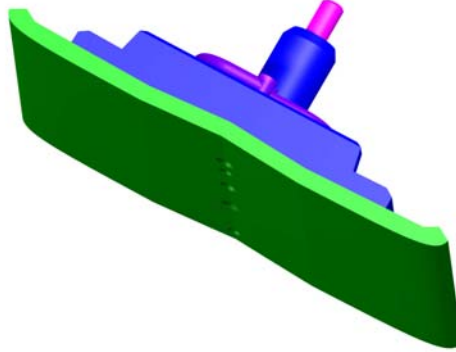


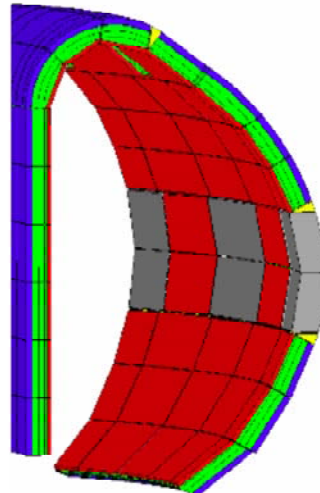
Figure 2. CAD model for the EHF FW14.

## II. CALCULATION APPROACH

The PARTISN [3] discrete ordinates code was used in X-Y geometry with S12 and ray tracing first collision source to mitigate ray effects. We used the reference ITER nuclear data library FENDL-2.1 [4] in 175 neutron-42 gamma energy groups. The poloidal variation of neutron wall loading in ITER based on a 3-D calculation with the exact source profile [5] is provided in Table I. The results for each BM were normalized to the corresponding neutron wall loading value at the associated poloidal location. We assumed that the modules are exposed to the full ITER average FW fluence of  $0.3 \text{ MW}\cdot\text{yr}/\text{m}^2$ . With the average ITER neutron wall loading of  $0.57 \text{ MW}/\text{m}^2$ , this corresponds to 0.526 full power years (FPY) of operation.

TABLE I. POLOIDAL VARIATION OF NEUTRON WALL LOADING

Blanket Module #	Average Neutron Wall Loading ( $\text{MW}/\text{m}^2$ )
1	0.270
2	0.430
3	0.565
4	0.567
5	0.433
6	0.270
7	0.264
8	0.336
9	0.380
10	0.418
11	0.544
12	0.629
13	0.693
14	0.728
15	0.736
16	0.713
17	0.625
18	0.514



Based on the CAD models for each FW panel, a simplified 2-D configuration was developed for the 2-D analysis. The 2-D models used for BM02 and BM14 are given in Figs. 3 and 4, respectively. The NHF FW in BM02 consists of four distinctive layers (Be, Cu layer, FW SS support, and FW beam). The thicknesses of these layers are 10, 27, 35, and 135.7 mm, respectively. The material composition for each zone is shown in Fig. 3. The overall toroidal width is 1362 mm and the beam width is 587.4 mm. The total thickness of BM02 is 450 mm. A 10 mm poloidal gap exists between modules at this inboard poloidal location.

The EHF FW in BM14 consists of four regions. These are the Be layer, the FW fingers, the FW support arm, and the FW beam. The thicknesses for these regions are 8, 28, 35, and 119 mm, respectively. The material composition for each zone is shown in Fig. 4. The overall toroidal width of BM14 is 1242 mm. In the toroidal half of the module, the beam zone has a toroidal width of 232 mm and the support arm is 220 mm wide. A 15 mm poloidal gap exists between modules at this outboard poloidal location. The total thickness of BM14 is 450 mm. Noticeable differences between these modules include an 8 mm Be layer in EHF modules compared to 10 mm in NHF modules. In addition, the EHF FW includes a FW support arm. The FW finger zone (that includes both the Cu and SS layers) in the EHF module is about half the thickness of the FW finger zone in the NHF module. Furthermore, the water content in the support arm and beam of the EHF module is about half that in the FW SS support and beam of the NHF module.

We performed 2-D neutronics calculations to determine nuclear heating in the FW and SB using these models. They represent half a module surrounded with reflecting boundaries. Half of the poloidal gap is included in the model. A uniform isotropic 14 MeV volumetric neutron source is used in front of the plasma facing side of the FW. A

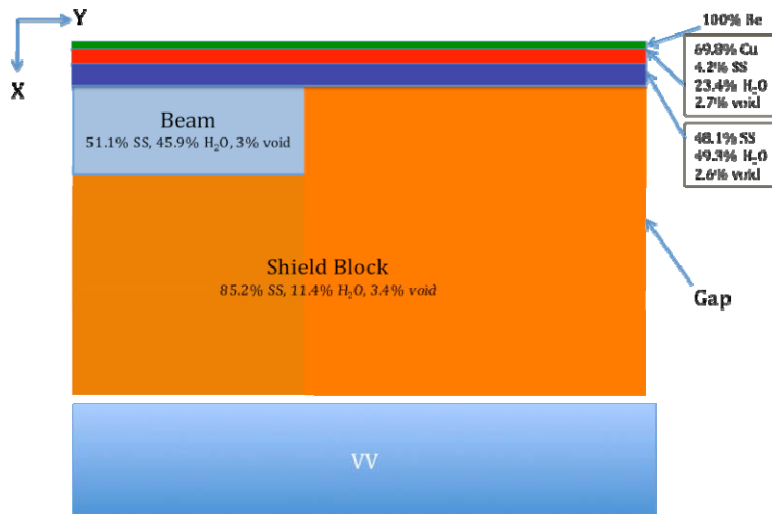


Figure 3. 2-D neutronics model for half of the NHF BM02.

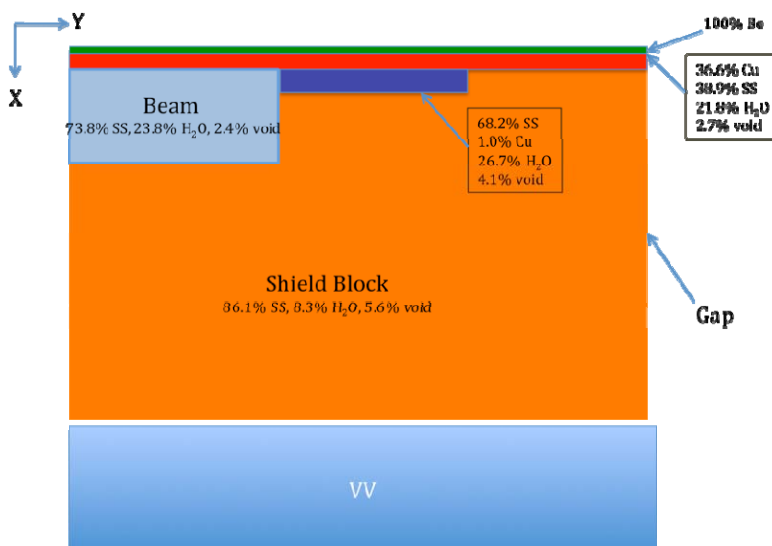


Figure 4. 2-D neutronics model for half of the EHF BM14.

reflecting boundary was utilized on the far side of the volumetric source to account for secondary neutrons and photons contributed from other blanket modules in the chamber. Nuclear heating and radiation damage profiles were determined in both toroidal (Y) and radial (X) directions. We used mesh elements that are at most 1 cm in width and average values were provided for each mesh element for each material existing there. Detailed tabulated results over this 2-D mesh were provided to be used as the source term for engineering analysis of these BM designs.

### III. RESULTS FOR BM02 WITH NHF FW PANEL

#### A. Nuclear Heating Profiles

Fig. 5 gives the nuclear heating as a function of depth in the NHF module BM02 at a section through the FW finger tip. The results for a section through the FW beam are given in Fig. 6. The toroidal variations of nuclear heating at different depths in BM02 are shown in Fig. 7. Only a minor impact of the poloidal gap is observed on nuclear heating at the front region of the FW with local heating (dominated by neutron heating) and a slight dip for Cu and SS (dominated by gamma heating). Local peaking in SS heating at the edge of the SB increases to  $\sim 1.5$  as one moves deeper toward the back of the SB of BM02. The dominant effect on heating profiles is the water distribution with larger SS nuclear heating (and slightly lower water heating) in the FW beam with large water content.

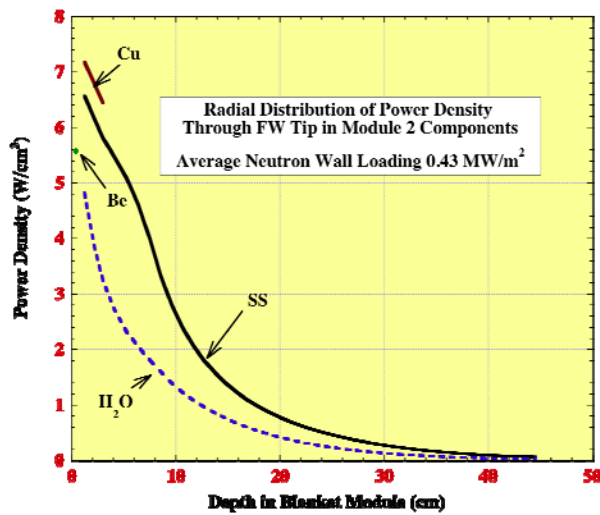


Figure 5. Nuclear heating at section through FW finger tip in BM02.

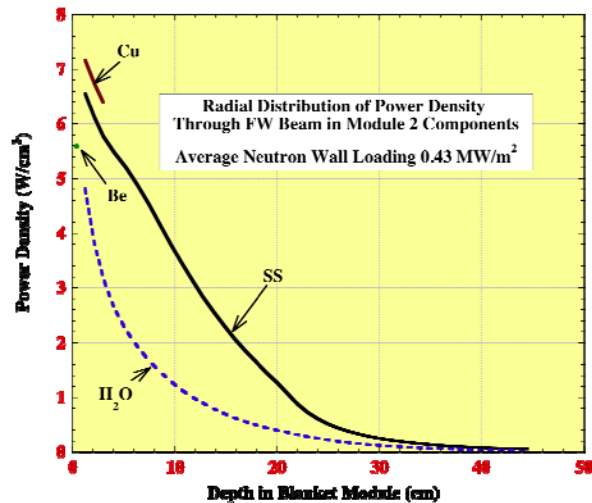


Figure 6. Nuclear heating at section through FW beam in BM02.

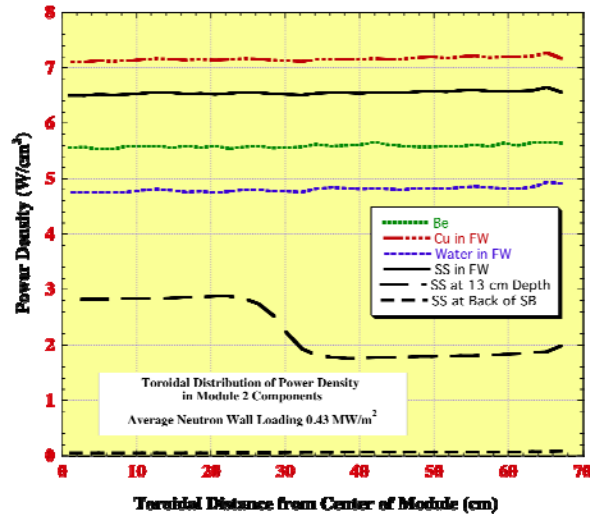


Figure 7. Toroidal variation of nuclear heating in BM02.

The toroidal nuclear heating profiles are nearly flat in the front regions of the FW. However, at the same radial depth through the beam, SS heating in the beam is larger by a factor of  $\sim 1.65$  than in the adjacent SB due to the large water content in the beam. This is also clear by comparing the radial distributions of nuclear heating in Figs. 5 and 6 where a noticeable bulge exists in SS heating in the FW beam. The water in the beam results in more gamma generation due to neutron moderation leading to larger heating in the SS. The impact of water on increasing steel heating in regions adjacent to it was discussed in detail in a previous analysis [6].

We calculated the total volume integrated nuclear heating in the SB and the different zones of the FW. The total heating in the FW is 0.589 MW (0.061, 0.216, 0.171, and 0.141 MW, in Be, Cu zone, SS support, and beam, respectively) and total heating in the SB is 0.264 MW. Total heating in the BM is 0.853 MW resulting in an energy multiplication factor of 1.46.

### B. Radiation Damage Profiles

Fig. 8 shows the radial profile of the end-of-life atomic displacements at several sections in BM02. Fig. 9 gives the results for helium production. The results indicate that the peak damage parameters in the front region of the FW are nearly uniform in the toroidal direction. The damage parameters drop radially by an order of magnitude in  $\sim 15$  cm with helium production dropping slightly faster. At the same radial location, the Cu dpa values are slightly ( $< 3\%$ )

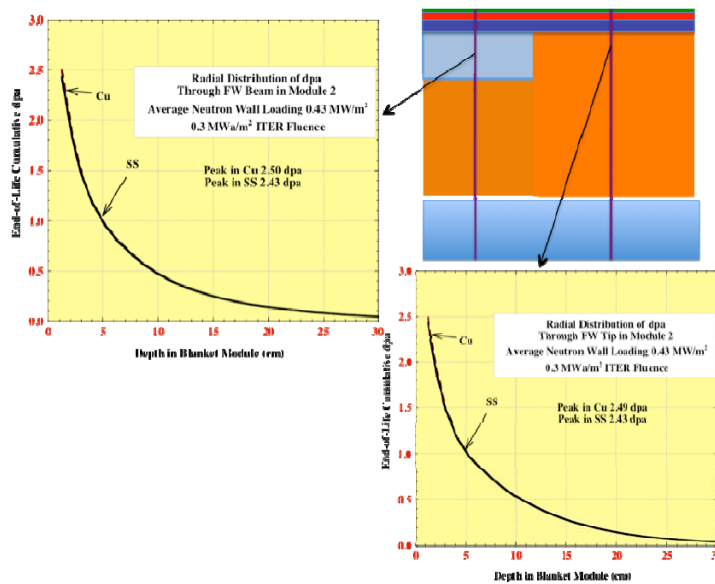


Figure 8. Radial distribution of dpa in BM02.

higher than the SS dpa values. On the other hand, at the same radial location, the SS helium production values are higher by up to ~50% than in Cu due to the existence of Ni (12.25%) and B (10 wppm) in the SS316L(N)-IG that have enhanced helium production by low energy neutrons.

The water content affects the dpa and helium production values in SS. The SS dpa values in regions with large water content are smaller due to the softer neutron spectrum. The dpa values in the beam are ~15% lower than those in the SB adjacent to it due to the softer neutron spectrum. The SS He production values in regions with large water content are enhanced due to production by low energy neutrons in Ni and B. The end-of-life He production drops to 3 appm (limit for thin plate and tube rewelding) at a depth of ~20 cm. The results imply that rewelding is possible only beyond this depth.

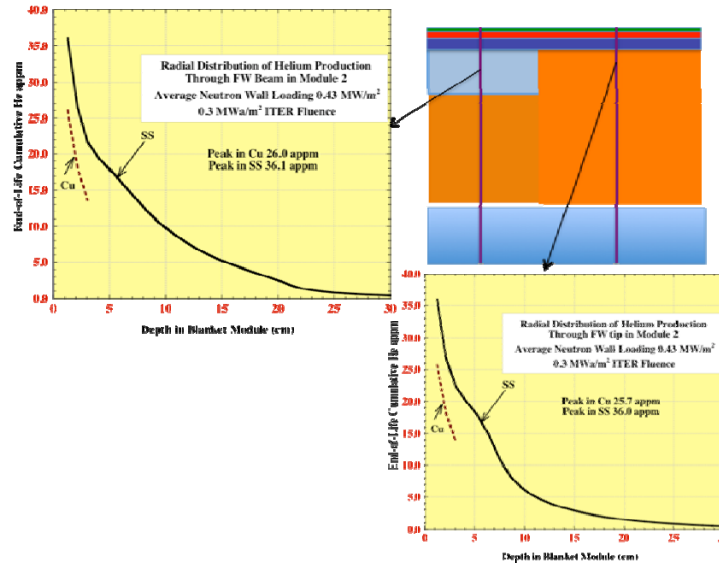


Figure 9. Distribution of helium production in BM02.

#### IV. RESULTS FOR BM14 WITH EHF FW PANEL

##### A. Nuclear Heating Profiles

Fig. 10 gives the nuclear heating as a function of depth in the EHF Module BM14 at a section through the FW beam. The results for a section through the FW support arm are given in Fig. 11 while Fig. 12 shows the results for a section through the FW fingers. The toroidal variations of nuclear heating at different depths in BM14 are shown in Fig. 13. Only a minor impact of the poloidal gap is observed on nuclear heating at the front region of the FW. Local peaking for SS at the edge of the SB increases to ~1.75 as one moves deeper towards the back of the SB of BM14.

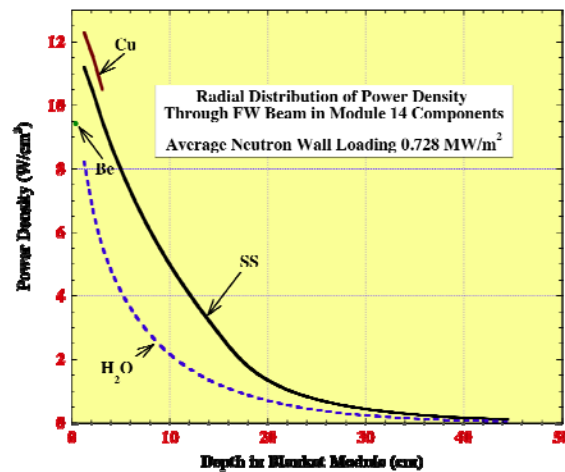


Figure 10. Nuclear heating at section through FW beam in BM14.

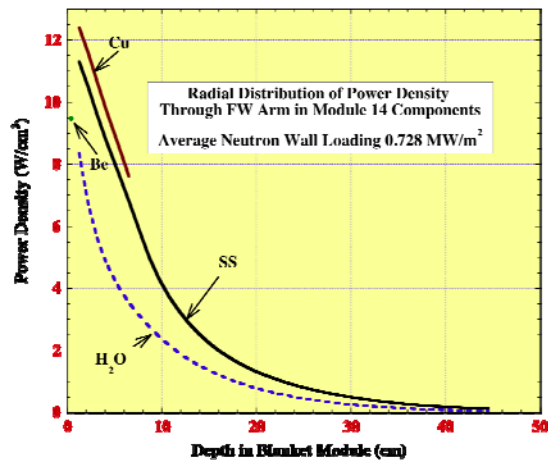


Figure 11. Nuclear heating at section through FW support arm in BM14.

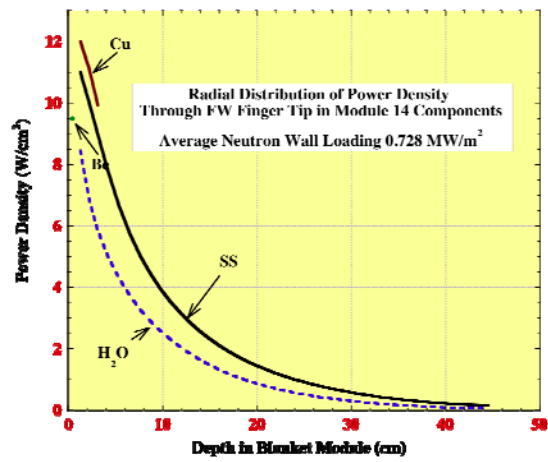


Figure 12. Nuclear heating at section through FW finger tip in BM14.

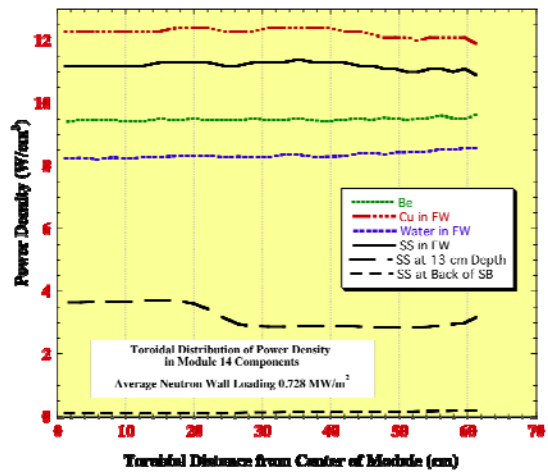


Figure 13. Toroidal variation of nuclear heating in BM14.

This peaking is higher than that obtained for the inboard BM02 that has a smaller poloidal gap. The dominant effect on heating profiles is the water distribution with larger SS nuclear heating (and slightly lower water heating) in the FW beam and support arm with larger water content than in adjacent SB.

At the same radial depth through the beam, SS heating in the beam is larger by up to a factor of ~1.3 than in the adjacent SB due to the large water content in the beam. This increase is lower than in the NHF modules that have larger water content in the beam. The total heating in the FW (including the beam) is 0.807 MW (0.097, 0.347, 0.102, and 0.261 MW, in Be, fingers, support arm, and beam, respectively) and total heating in the shield block is 0.543 MW. Total heating in the FW and shield block is 1.35 MW resulting in an energy multiplication factor of 1.45.

### B. Radiation Damage Profiles

Fig. 14 shows the radial profile of the end-of-life atomic displacements at several sections in BM14. Fig. 15 gives the results for helium production. The results indicate that the peak damage parameters in the front region of the FW are nearly uniform in the toroidal direction with slight increase at edge of the finger. The damage parameters drop radially by an order of magnitude in ~15 cm with helium production dropping slightly faster. At the same radial location Cu and SS dpa values are comparable with ~3% higher values in Cu. On the other hand, at the same radial location, the SS helium production values are higher by up to ~50% than in Cu due to enhanced production in Ni and B existing in the SS316L(N)-IG.

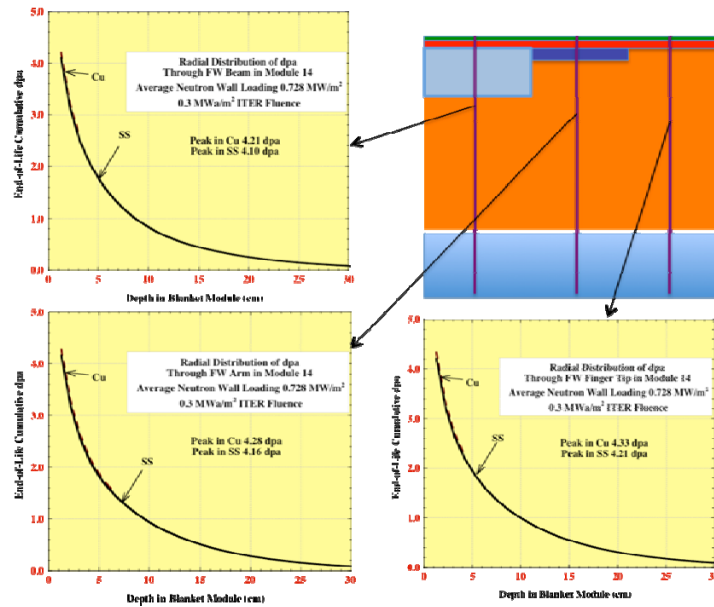


Figure 14. Radial distribution of dpa in BM14.

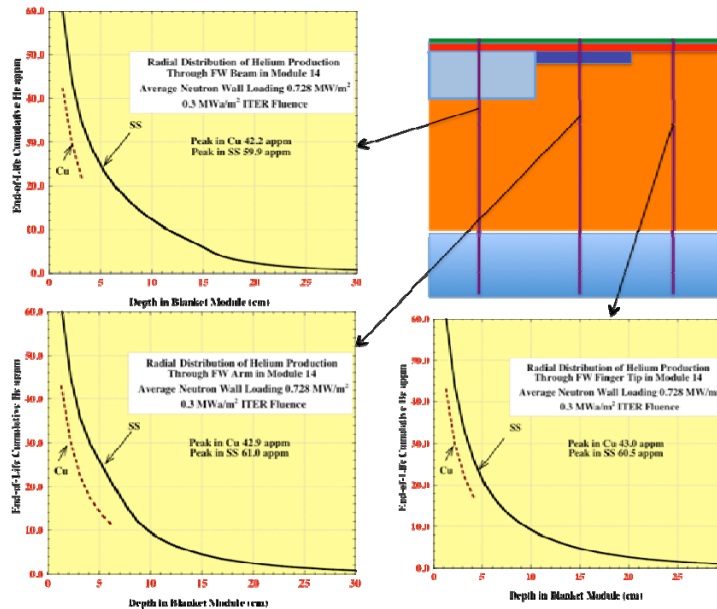


Figure 15. Distribution of helium production in BM14.

The SS dpa values in regions with large water content are smaller due to the softer neutron spectrum. The dpa values in the beam are ~8% lower than those in the SB adjacent to it which is not as pronounced as that observed for the NHF modules (~15%) with larger water content in the beam. The SS He production values in regions with large water content are enhanced due to production by low energy neutrons in Ni and B. We observe higher SS He production values in regions with large water content (by ~35%) compared to those in adjacent SB. This effect is not as pronounced as in the NHF modules (~60%). The end-of-life He production drops to 3 appm (limit for thin plate and tube rewelding) at a depth of ~19 cm in BM14. The results imply that rewelding is possible only beyond this depth in the blanket module.

Several of the 18 blanket modules at poloidal location 14 between equatorial ports have flat NHF FW panels shown in Fig. 16. These modules are designated BM14F. We generated the 2-D nuclear heating and radiation damage results for the NHF module BM14F and compared the results to those for the EHF module BM14 at the same poloidal location.

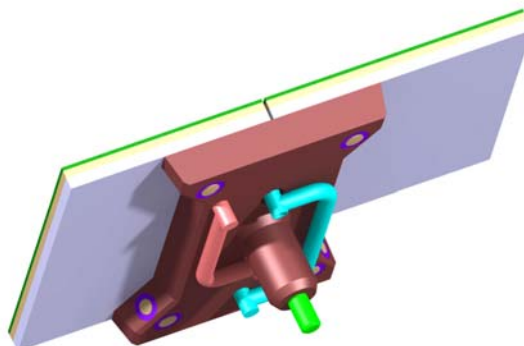


Figure 16. CAD model for BM14F.

It is interesting to compare the nuclear heating radial profiles in modules BM14 and BM14F that have the same neutron wall loading. Fig. 17 shows the comparison for SS nuclear heating. We observed lower SS and Cu heating in the Cu layer of the fingers of the NHF FW14F due to the lower water content (only 13.7%) in this layer. Much larger SS heating occurs in the FW SS support and FW beam due to nearly twice the water content in the NHF module. The peaking in SS nuclear heating in the beam compared to the adjacent SB is significantly larger (1.75 in BM14F vs. 1.3 in BM14).

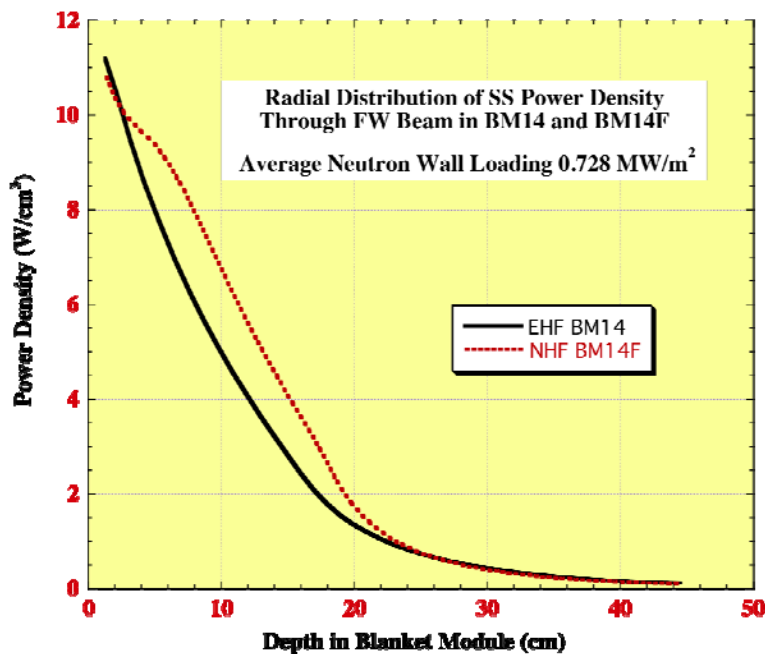


Figure 17. SS nuclear heating profiles in BM14 and BM14F.

Figs. 18 and 19 compare the SS dpa and He production profiles in BM14 and BM14F. We observe lower SS dpa in the FW SS support and FW beam of BM14F due to the larger water content that yields a softer neutron spectrum. On the other hand, a much larger SS helium production results in the FW SS support and FW beam of BM14F due to nearly twice the water content that results in enhanced helium generation by low energy neutrons in B and Ni.

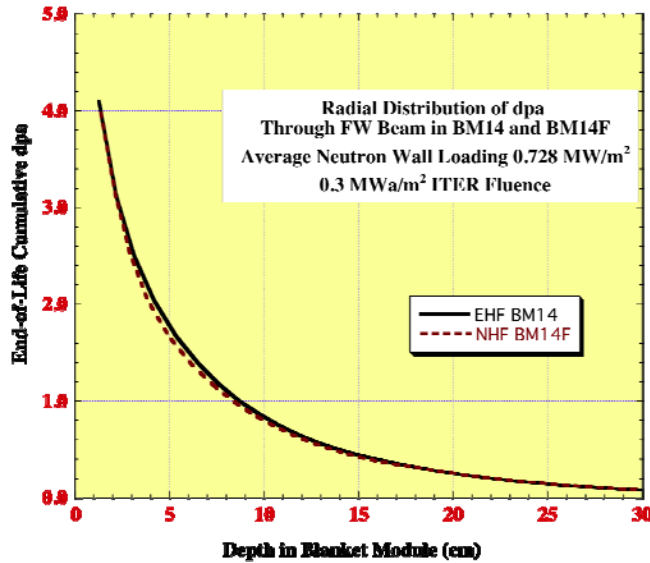


Figure 18. Comparison between SS dpa profiles in BM14 and BM14F.

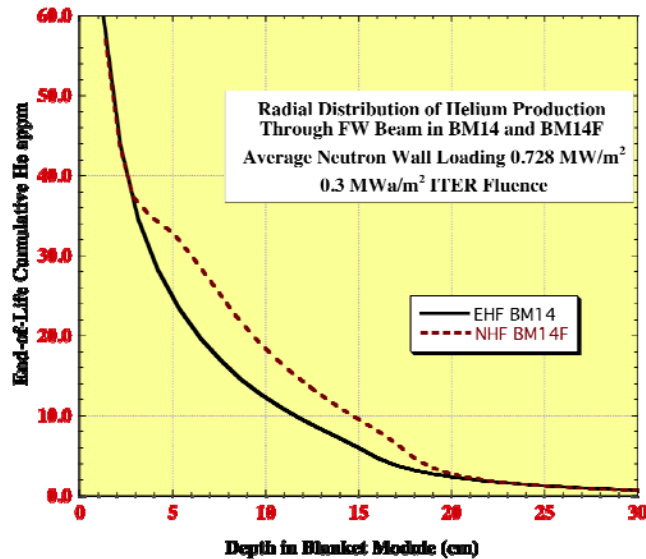


Figure 19. SS He production profiles in BM14 and BM14F.

## V. CONCLUSIONS

Detailed profiles of nuclear heating were determined for each constituent material (Be, CuCrZr, SS316L(N)-IG, and H<sub>2</sub>O) in the EHF and NHF ITER blanket modules using 2-D models. Tabulated results were provided over a fine 2-D mesh to use for engineering analyses and help evaluating the FW design options. These profiles are significantly impacted by the variation in water content in the different zones of the FW and SB with larger SS heating in zones with larger water content due to enhanced gamma generation. The results indicate that the peak damage parameters in the front region of the FW are nearly uniform in the toroidal direction in each module. The damage parameters drop radially by an order of magnitude in ~15 cm with helium production dropping slightly faster. At the same radial location, the Cu and SS dpa values are comparable while the SS helium production values are higher than in Cu due to the existence of Ni and B in the SS316L(N)-IG. The SS helium production values in regions with large water content are enhanced due to production by low energy neutrons in B and Ni.

The main problem with the 2-D analysis is that the source distribution is assumed to be uniform in the plasma zone compared to the actual ITER source distribution. This introduces an overestimate for heating and other nuclear parameters in the front zones of the FW (<30%) but good agreement as we move into the BM [7]. While these 2-D profiles are useful for quick evaluation of the different BM design options, detailed 3-D analysis using the CAD-based Monte Carlo code (DAG-MCNP) [8] will be performed as the project proceeds to a reference design. The detailed CAD models for each individual module will be inserted in the most recent global ITER model with the accurate source profile to determine a high-resolution map of nuclear heating using a fine mesh.

#### ACKNOWLEDGMENT

This paper was prepared as an account of work by or for the ITER Organization. The Members of the Organization are the People's Republic of China, the European Atomic Energy Community, Republic of India, Japan, Republic of Korea, the Russian Federation, and the United States of America. The views and opinions expressed herein do not necessarily reflect those of the Members or any agency thereof. Dissemination of the information in this paper is governed by the applicable terms of the ITER Joint Implementation Agreement. This work was sponsored in part by the US ITER Organization through Sandia National Laboratories.

#### REFERENCES

- [1] M. Merola, D. Loesser, A. Martin, P. Chappuis, et al., "ITER Plasma-facing components," *Fusion Engineering & Design*, vol. 85, pp. 2312-2322, 2010.
- [2] R. Mitteau, P. Stangeby, C. Lowry, M. Merola, et al., "Heat loads and shape design of the ITER first wall," *Fusion Engineering & Design*, vol. 85, pp. 2049-2053, 2010.
- [3] R.E. Alcouffe, R.S. Baker, J.A. Dahl, S.A. Turner, and Robert Ward, "PARTISN: A Time-Dependent, Parallel Neutral Particle Transport Code System," LA-UR-05-3925, Los Alamos National Laboratory (May 2005).
- [4] D.L. Aldama and A. Trkov, "FENDL-2.1, Update of an Evaluated Nuclear Data Library for Fusion Applications," Report INDC(NDS)-467, International Atomic Energy Agency (2004).
- [5] P. Wilson et al., "State of the art 3-D radiation transport methods for fusion energy systems," *Fusion Engineering & Design*, vol. 83, pp. 824-833, 2008.
- [6] T.D. Bohm, M.E. Sawan, B. Smith, and P.P.H. Wilson, "Peaking in SS Nuclear Parameters at Water Interface," University of Wisconsin Fusion Technology Institute, UWFDI-1376 (2009).
- [7] B. Smith, P. Wilson, M. Sawan and T. Bohm, "Source profile analysis for the ITER first wall/shield modules," *Fusion Science & Technology*, vol. 56, pp 57-62, 2009.
- [8] T. Tautges, P.P.H. Wilson, J. Kraftcheck, B. Smith, and D. Henderson, "Acceleration Techniques for Direct Use of CAD-Based Geometries in Monte Carlo Radiation Transport," *Proceedings of International Conference on Mathematics, Computational Methods & Reactor Physics (M&C 2009)*, Saratoga Springs, New York, May 3-7, 2009.